JOURNAL OF AIRCRAFT
Vol. 41, No. 4, July–August 2004

Drag Reduction from Square-Base Afterbodies at High Speeds

N. B. Mathur* and P. R. Viswanath†
National Aerospace Laboratories, Bangalore 560 017, India

Experiments have been carried out in the 0.5-m base flow wind tunnel at high speeds evaluating the drag reduction potential of a family of square base afterbodies including jet flow at the base. Direct afterbody total drag measurements have been made on square bases as well as conventional axisymmetric afterbodies with conical and circular arc boat tails having the same annular base area and jet flow parameters. The results show conclusively that, in the Mach-number range of 0.95–1.60, the square-base afterbodies have globally minimum drag in the range of jet pressure ratio studied; the total drag reduction observed is about 10–12% relative to the circular arc afterbodies, which can be of significant value in design applications. Certain broad flow features on square-base afterbodies are discussed based on surface-pressure measurements and surface flow-visualization studies.

Nomenclature

A_b	=	annular base area
A_b/A_f	=	ratio of annular base area to forebody area, 0.23
A_f	=	forebody cross-sectional area
A_j	=	area of jet at exit
A_j/A_f	=	ratio of jet exit area to forebody area, 0.30
C_D	=	afterbody total drag coefficient; drag force/$(q_{\infty *}A_f)$
C_{Db}	=	base-drag coefficient; base force/$(q_{\infty *}A_f)$
$C_{D\beta}$	=	boat-tail profile drag coefficient; boat-tail drag force/$(q_{\infty *}A_f)$
C_p	=	afterbody surface-pressure coefficient; $(p - p_\infty)/(0.5\gamma p_\infty M_\infty^2)$
C_{pb}	=	base-pressure coefficient; $(p_b - p_\infty)/(0.5\gamma p_\infty M_\infty^2)$
D	=	forebody diameter of the model, 127 mm
d_b	=	base diameter
d_j	=	nozzle-exit diameter
M_∞	=	freestream Mach number
P_{oj}/p_∞	=	jet pressure ratio; ratio of stagnation pressure of jet to the freestream static pressure
p_b	=	base pressure
p_∞	=	freestream static pressure
q_∞	=	dynamic pressure $(0.5\gamma p_\infty M_\infty^2)$
β	=	boat-tail angle, see Fig. 3

I. Introduction

THERE is significant interest in the use of a nonaxisymmetric afterbody in the context of future combat aircraft and missile applications.[1,2] Nonaxisymmetric afterbody-nozzle (including two-dimensional) incorporating thrust-vectoring concepts are being seriously considered[3,4] for futuristic aircraft for attaining low drag and increasing combat effectiveness. Afterbodies of such design will be necessarily three-dimensional, as well as those of twin-engine configurations. The database on drag characteristics of three-dimensional afterbodies is in general sparse and guiding principles for their designs are virtually nonexistent.

In this paper, we have investigated the zero-lift drag characteristics of a class of square-base afterbodies including jet effects at high speeds. The square-base afterbody is generated by cutting an axisymmetric cylinder symmetrically by four planes inclined at an angle β (with respect to cylinder axis) (Fig. 1); this results in four inclined flat segments with a square cross section at the base. The flow features on the flat segments involve vortices[5,6] similar to those on a sharp leading edge delta wing at an incidence (equal to β). The zero-lift drag characteristics of the preceding class of square-base afterbodies in the absence of jet flow have been studied,[5–7] and such a design has been considered[7] in contemporary missile and projectile applications because they offer other aerodynamic benefits (e.g., increased lift-curve slope at supersonic speeds).

A systematic experimental study has been carried out to examine behaviour of jet–freestream interaction causing changes in afterbody drag characteristics of square-base afterbodies at transonic and low supersonic speeds. The drag characteristics of these square-base afterbodies are compared with conventional axisymmetric counterpart involving circular arc and conical boat tails having the same base area and jet flow parameters. The drag-reduction potential and certain flow features of square-base afterbodies are discussed in this paper.

II. Experiments

A. Experimental Facility and Afterbody Models

Experiments were carried out in the 0.5-m base flow facility (Fig. 2), a special purpose blowdown-type tunnel that was commissioned during 1991; the basic design features of the tunnel were procured from AMRAD International Corporation. Some of the special features of this tunnel are 1) axisymmetric variable geometry nozzle, which can provide test Mach numbers in the range of 0.4 to 3.5 (unit Reynolds number in the range of $10–50 \times 10^4$/m); 2) the models are supported directly on the nozzle innerbody (Fig. 2), and therefore the support system interference is completely eliminated; 3) fairly well-developed zero-pressure-gradient turbulent boundary-layer characteristics on the afterbody; and 4) easier mounting and changing of the afterbody-nozzle models. The facility is being extensively used for afterbody and base flow research with jet flow simulation using air at ambient total temperature conditions.

The tunnel has been extensively calibrated, and the results[8] indicate good mean flow uniformity and axisymmetry of the freestream and jet flow in the tunnel. The measured afterbody surface and base pressure distributions on standard cylindrical and boat-tailed afterbody models (e.g., Royal Aircraft Establishment, NASA and AGARD models) showed good agreement[8] with published results in literature. The boundary layer approaching the nonmetric/metric section of the afterbody model is turbulent, and the ratio of boundary-layer thickness to the forebody diameter varies[9] from about 4 to 6.5% in the freestream Mach-number range of 0.8–1.6 of this investigation; the mean velocity profiles display a logarithmic region (with the slope and intercept having values typical of compressible turbulent boundary-layer flow), suggesting a fairly well-developed turbulent boundary layer approaching the afterbody.

For this parametric study, three families of afterbodies with different boat-tail angles and employing a sonic nozzle were designed

Received 3 February 2003; revision received 28 November 2003; accepted for publication 28 November 2003.

*Deputy Director, Experimental Aerodynamics Division.
†Head, Experimental Aerodynamics Division. Associate Fellow AIAA.

as shown in Fig. 3. All of the afterbodies (Figs. 3a–3c) designed have the same ratio of annular base area to forebody area (A_b/A_f) of 0.23 and jet-exit area to forebody area (A_j/A_f) of 0.30 so that direct comparison of drag characteristics of afterbody with square and axisymmetric base could be made.

B. Direct Afterbody Drag Measurement Technique

Afterbody drag in the presence of jet flow is measured using a special three-component annular strain-gauge balance system (Fig. 4) having the following load capacity of balance elements: axial force, 20 kgf; normal force, 40 kgf; and pitching moment, 120 kg-cm. The drag measurement technique[10] used is similar to those employed in literature for the measurement of afterbody forces (e.g., Refs. 1–3, 5, and 6). The metric afterbody is separated from the nonmetric forebody by an annular gap (Fig. 4) and sealed with a soft Teflon® ring (which prevents transfer of axial forces). The balance does not measure the jet forces because the balance is grounded through the jet pipe. An important feature of this measurement system is that internal corrections (generally required to correct balance axial force output in this type of measurements) are relatively small and need only the measurements of static pressures in the model cavity and split-seal regions for the accurate determination of afterbody drag.[8] This strain-gauge balance has been successfully used in a variety of experimental investigations.[10]

C. Instrumentation

Metric/nonmetric interface region of the model assembly (see Fig. 2) was provided with four pressure tapings at equally spaced circumferential locations for the measurement of static pressure in the split-seal region; eight pressure tapings were provided in the annular cavity (between the external surface of the nozzle and

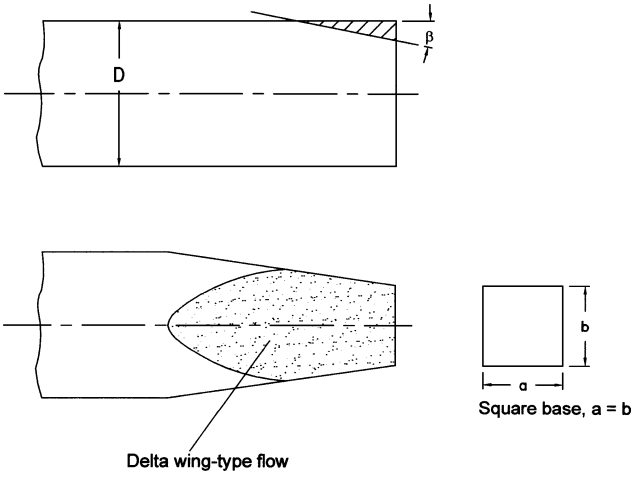

Fig. 1 Geometric details of a square-base afterbody.

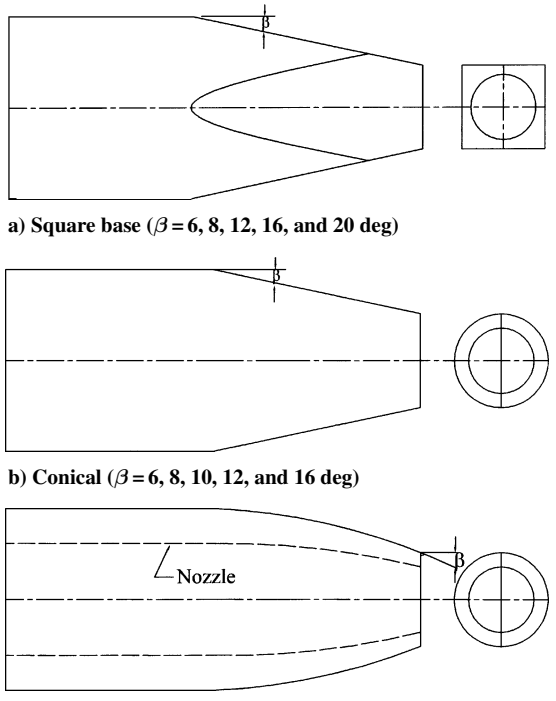

a) Square base ($\beta = 6, 8, 12, 16$, and 20 deg)

b) Conical ($\beta = 6, 8, 10, 12$, and 16 deg)

c) Circular-arc ($\beta = 6, 9, 12, 16$, and 20 deg)

Fig. 3 Sketch of afterbody configurations.

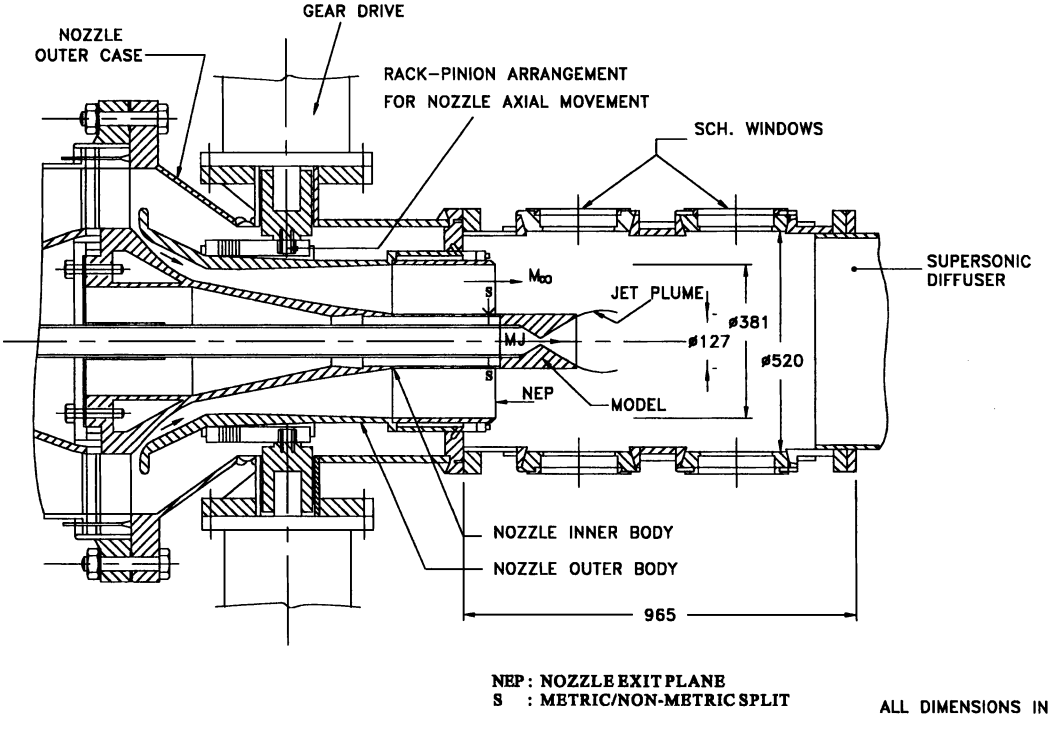

Fig. 2 Variable geometry axisymmetric nozzle test-section assembly of base flow wind tunnel.

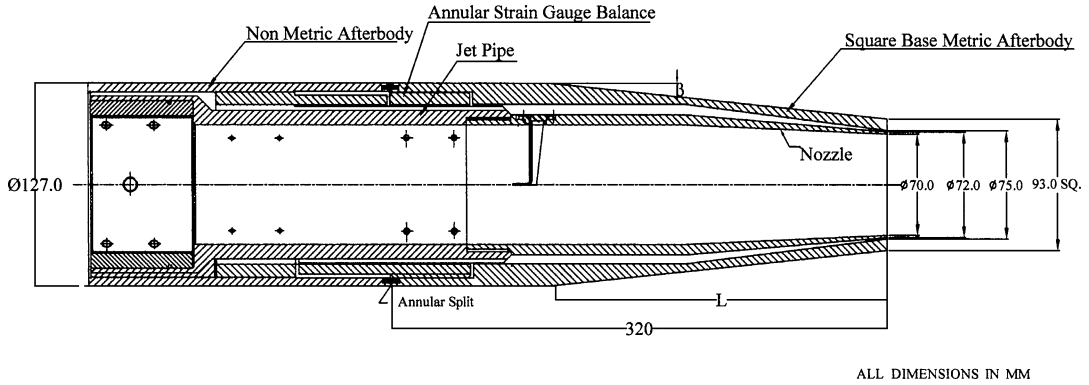

Fig. 4 Direct measurement of afterbody drag with jet flow: annular strain-gauge balance—square-base afterbody assembly.

inside of the afterbody model) at different streamwise and circumferential locations to provide a good average of cavity pressure. The base pressure was vented into the annular cavity (Fig. 4), and so the measured cavity pressure is also the base pressure on the afterbody model. Static pressures in the cavity and split-seal regions were measured using a 68.95 kn/m^2 electronic pressure scanner (ESP). To gain some insight on typical flow features on the square-base afterbody, spanwise and streamwise surface-pressure distributions were measured on a square-base afterbody configuration having $\beta = 8$ deg. There were 12 streamwise static-pressure ports (i.d. of 0.8 mm) along the centerline and 19 static-pressure tapings in the spanwise direction; a large number of static-pressure tapings in the spanwise direction were provided to capture the features of vortex flow along with jet–freestream interaction flow phenomenon. Freestream total and static pressures were measured using DRUCK pressure transducers of range ±689.5 and 68.95 kn/m,^{2} respectively. For this investigation, jet flow was at the exit sonic, and this was ascertained from the measurements of jet total pressure at the nozzle entry and jet static pressure at the exit of the nozzle. Jet stagnation and static pressures of the convergent nozzle were measured using DRUCK pressure transducers of the range 0–1379 and ±68.95 kn/m,^{2} respectively. All of the pressure sensors were calibrated in situ using a Texas Instruments master pressure gauge. The forces measured by the three-component annular strain-gauge balance system and all of the pressures were acquired through the different channels of a Pentium-based data-acquisition system.

D. Test Program

The wind-tunnel experiments were carried out in the freestream Mach-number range of 0.60–1.60, and the tunnel stagnation pressure varied between 115–225 kn/m^2 in the preceding Mach-number range; the corresponding Reynolds number per meter varied between 10–20 $\times 10^6$ at $M_\infty = 0.60$ and 1.60, respectively. The jet pressure ratio was varied in the range of 1–6; the sonic nozzle flow for these experiments was simulated using room-temperature air in the total pressure range of 115–415 kn/m^2 and total temperature of 300°K. Total drag measurements were made on three families of afterbody configurations having boat-tail angles in the range of 6 to 20 deg (Fig. 3). Measurements made included 1) afterbody drag in the presence of jet flow on square base, coical, and circular arc boattailed afterbodies and 2) longitudinal and spanwise surface-pressure distributions on a square-base afterbody model ($\beta = 8$ deg). In addition, surface flow-visualization studies were carried out specially on selected square-base afterbodies employing a mixture of titanium dioxide in oil.

E. Estimate of Uncertainty in Measured Data

All of the pressure sensors were frequently calibrated using a Texas Instruments master gauge. With regard to the afterbody drag measurements, the axial force measured by the balance was in the range of about 2–12 kg (which implied 10 to 60% of the balance axial-force capacity of 20 kgf), depending on the Mach number and

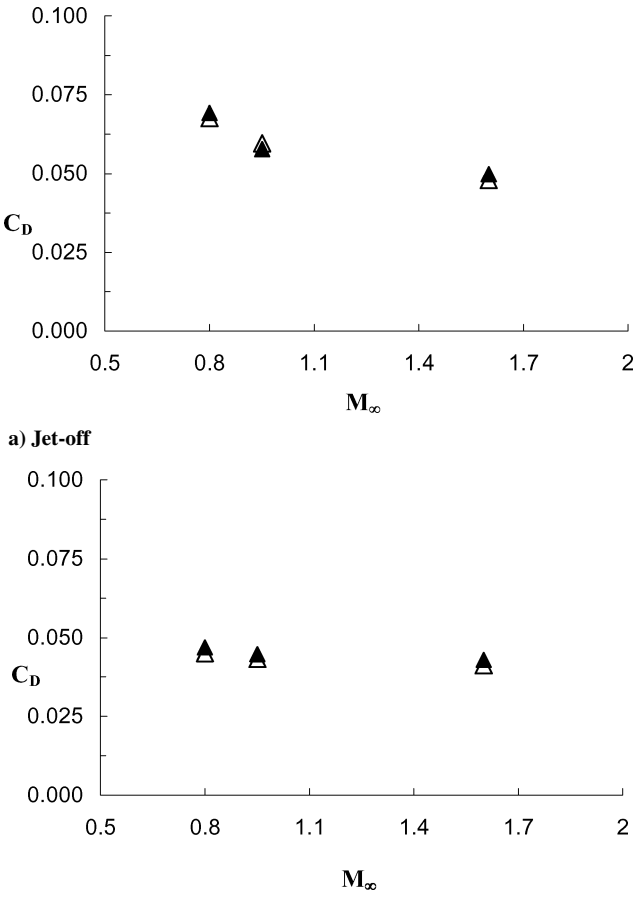

Fig. 5 Repeatability of drag data with and without jet flow: square-base afterboby ($\beta = 8$ deg).

afterbody-nozzle configurations. Hence the afterbody drag could be measured quite accurately with the axial-force capacity of this strain gauge balance used for these measurements. Measured axial-force output was corrected for the metric/nonmetric and model cavity pressures, and these corrections were in the range of 10–25% of the balance axial-force output. Wind-tunnel test data obtained from different blowdowns under the same flow conditions were checked for their repeatability. This was studied through the measurements of afterbody drag with and without the presence of jet flow for the same setting of freestream Mach number. Figures 5a and 5b show typical test results and the differences in afterbody drag as measured from different test blowdowns under the same flow conditions are well within 5%, indicating good repeatability of the test data in the entire test Mach-number range of this investigation. Taking into account calibration errors and repeatability of data, estimated

uncertainties are $\Delta C_D < \pm .05 C_D$ (20 to 1) and $\Delta C_p < \pm .02 C_p$ (20 to 1).

III. Results and Discussion

A. Afterbody Total Drag Characteristics

Typical effects of jet flow on afterbody drag characteristics of square base as well as on axisymmetric afterbodies with conical and circular arc boat-tails configurations are shown in Figs. 6–8 at $\beta = 6$, 8, and 12 deg, respectively; data at higher β of 16 and 20 deg are not included here because the drag levels were generally higher. It can be noted in Fig. 7 that drag comparisons are made at $\beta = 8$ deg for square-base and conical afterbodies while $\beta = 9$ deg for the circular arc; this was the closest and best comparison that could be attempted to bring out the relative merits, and a further discussion of this aspect follows in Sec. 3.B. These results (Figs. 6–8) provide direct comparison of jet-on-drag characteristics indicating the behavior of jet–freestream interactions causing changes in afterbody drag with the changes in jet pressure ratio. For conical and square-base afterbodies at high subsonic freestream Mach numbers ($M_\infty \leq 0.9$), the variation of afterbody drag with jet pressure ratio shows a similar trend, that is, in general

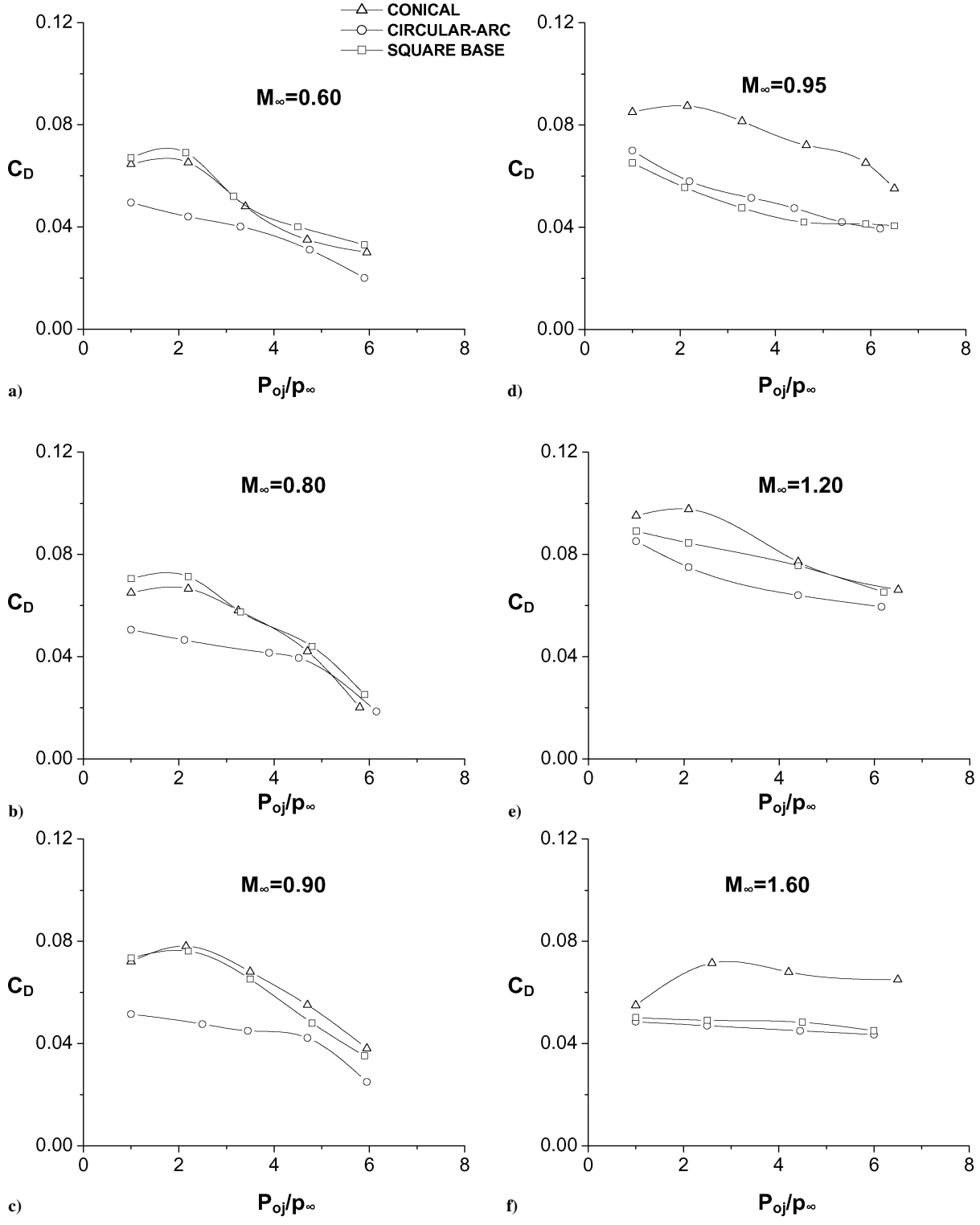

Fig. 6 Afterbody total drag characteristics at different Mach numbers: $\beta = 6$ deg.

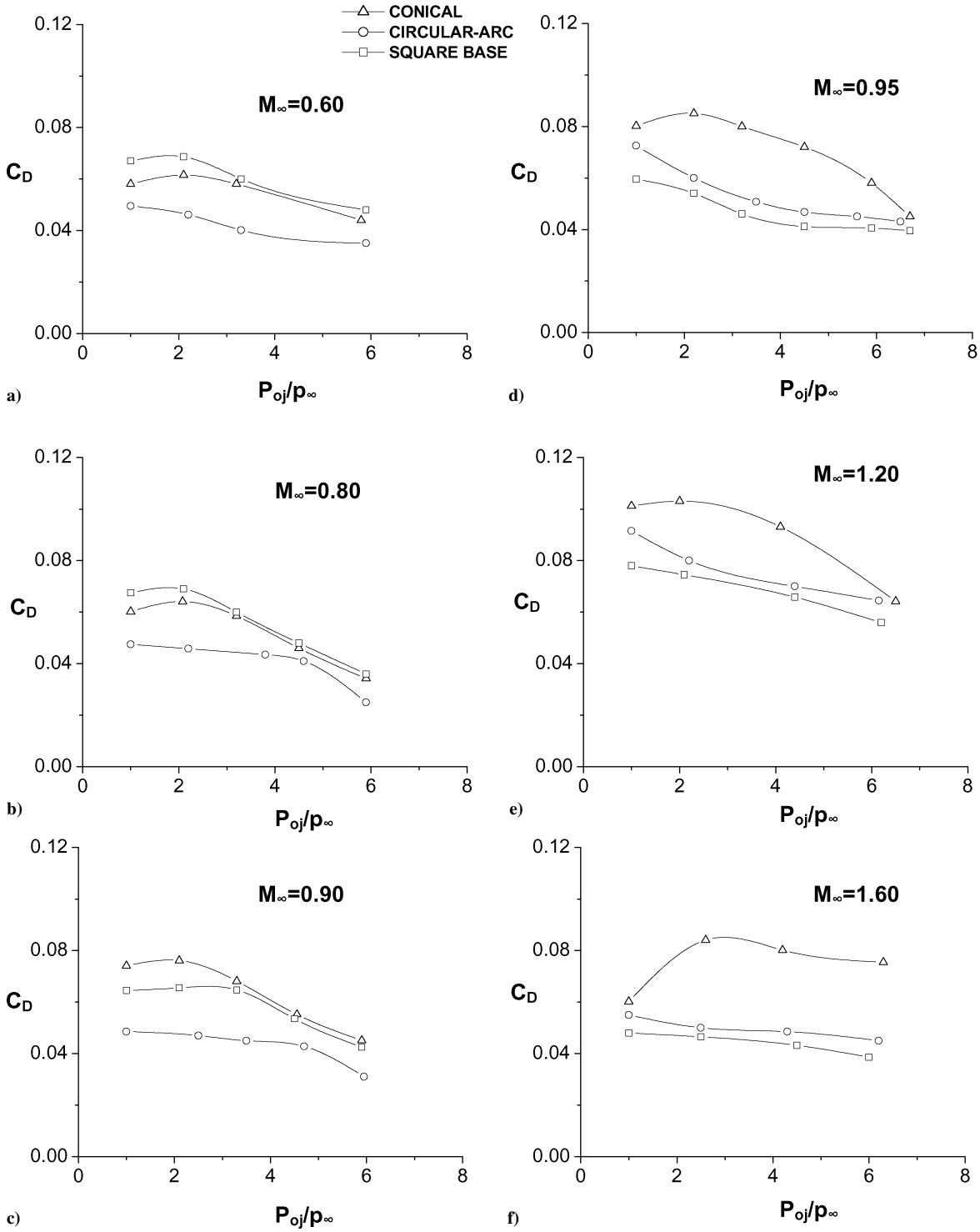

Fig. 7 Afterbody total drag characteristics at different Mach numbers: $\beta = 8$ deg.

a slight increase in the afterbody drag (upto $P_{oj}/p_\infty \approx 2$) and subsequent decrease with increase in jet pressure ratios. These results clearly indicate the favorable effect of jet–freestream interactions when the jet plume displacement effects become significant beyond jet pressure ratio of about two. Circular-arc boat-tailed afterbodies generally show a decreasing trend of afterbody drag with jet pressure ratio (Figs. 6a–6c, 7a–7c, 8a–8c). It is evident that lowest total drag is offered by circular-arc boat-tailed afterbodies at high subsonic Mach numbers of 0.60, 0.80, and 0.90 because of gradually expanding flow and the optimum boat-tail angle is 9 deg. However, it is interesting to note from Figs. 7d–7f that, at $M_\infty = 0.95$, 1.20, and 1.60, the afterbody drag of square base with $\beta = 8$ deg is even lower than that of corresponding circular-arc boat-tailed afterbody. We shall discuss these aspects further in Sec. 3.B.

B. Minimum Total Afterbody Drag Characteristics

Having observed the drag-reduction potential of square-base afterbody with $\beta = 8$ deg at the higher Mach numbers, the total drag characteristics of square-base and circular-arc afterbodies at different β (around the optimum) are compared in Figs. 9–11, in order to identify the afterbody of minimum total drag (in a global sense) at Mach numbers of 0.95, 1.20, and 1.60; results from conical

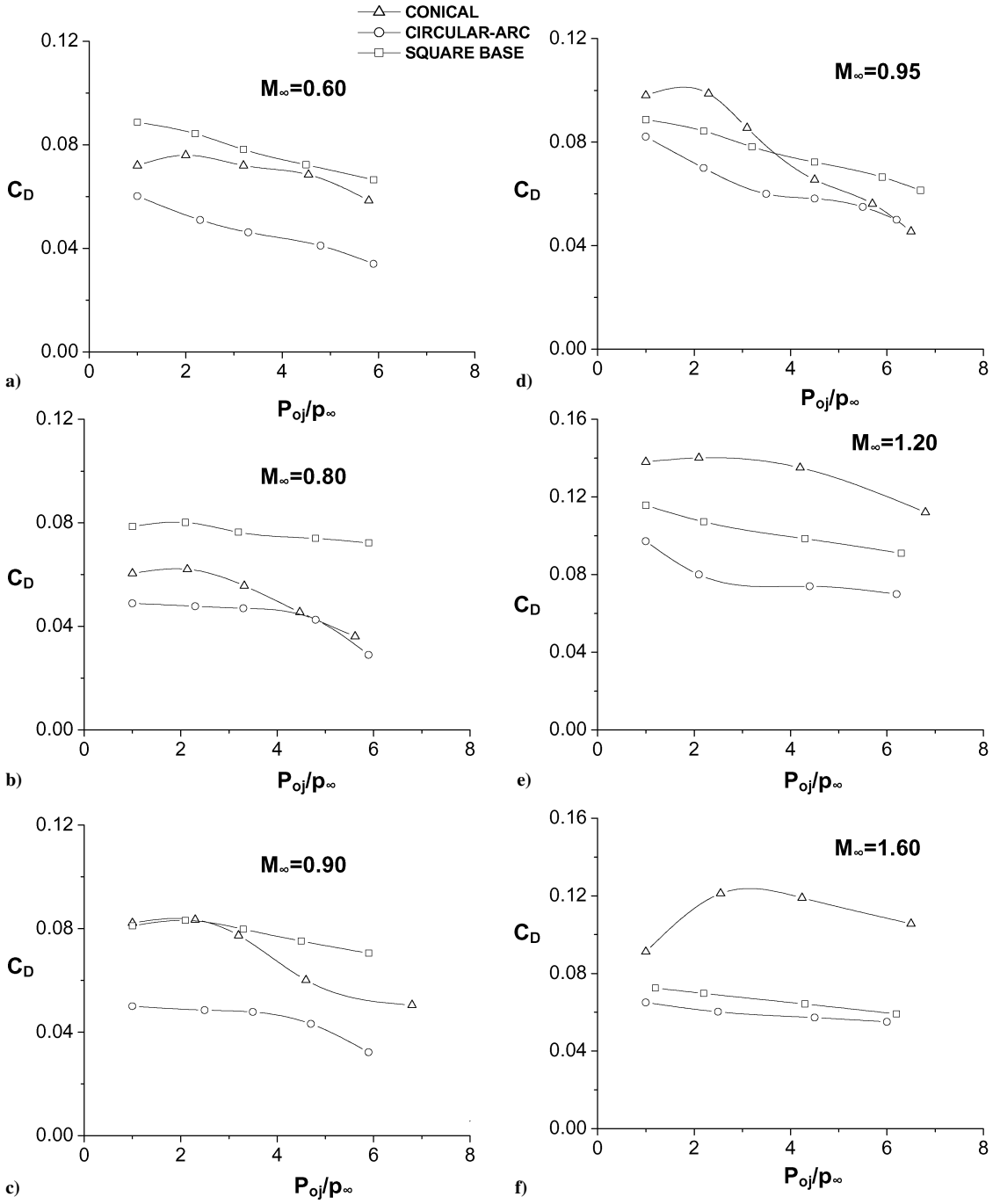

Fig. 8 Afterbody total drag characteristics at different Mach numbers: $\beta = 12$ deg.

boat tails are not included in the preceding figures because they have the highest drag. These results explicitly show (Figs. 9–11) that the lowest drag is offered by the square-base afterbody, and in particular, the drag value of the circular-arc boat tail at $\beta = 8$ deg (interpolated) is generally higher than the square base with $\beta = 8$ deg.

In summary, at $M_\infty = 0.6$, 0.8, and 0.90, the circular-arc afterbody has the lowest total drag, whereas at higher M_∞ of 0.95, 1.20, and 1.60, the square-base afterbody with $\beta = 8$ deg has the lowest total drag across the jet pressure ratio as shown in Fig. 12. The net total drag-reduction offered by the square base with $\beta = 8$ deg is about 10–12% compared to circular-arc boat tails (Figs. 9–11). It seems likely that the vortex flow generated on the flat segments[5,6] of the square-base afterbodies (qualitatively similar to those on a sharp leading-edge delta wing at incidence) energize the boundary-layer flow of the afterbody (like a vortex generator in the board sense), thereby providing a greater resistance to the plume-induced boundary-layer separation on the afterbody and therefore a lower transonic drag rise (particularly at higher transonic Mach numbers).

C. Components of Afterbody Drag

Having observed the drag benefits of square-base afterbodies, it is relevant and appropriate to assess which component of the total afterbody drag is resulting in net drag reduction on such bodies. The two major components of afterbody drag are the boat-tail profile drag $C_{D\beta}$ and base-drag coefficient C_{Db}: the base area being same for all of the afterbodies, the base pressure coefficient C_{pb} provides the same information as base-drag coefficient C_{Db}. The boat-tail profile drag (for each flow condition) is obtained by subtracting the base-drag contribution from the measured total drag C_D. In Figs. 13a–13c, the two components of total afterbody drag, namely, $C_{D\beta}$ and C_{Db} corresponding to the minimum total drag conditions for

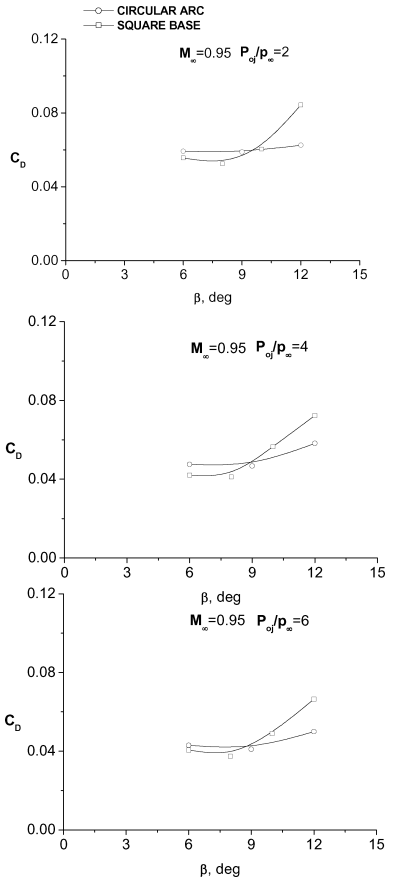

Fig. 9 Comparison of total drag characteristics of circular-arc and square-base afterbodies: $M_\infty = 0.95$.

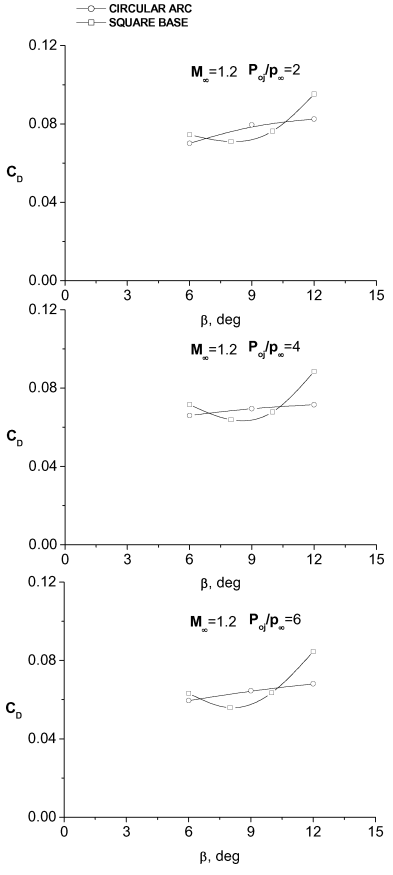

Fig. 10 Comparison of total drag characteristics of circular-arc and square-base afterbodies: $M_\infty = 1.20$.

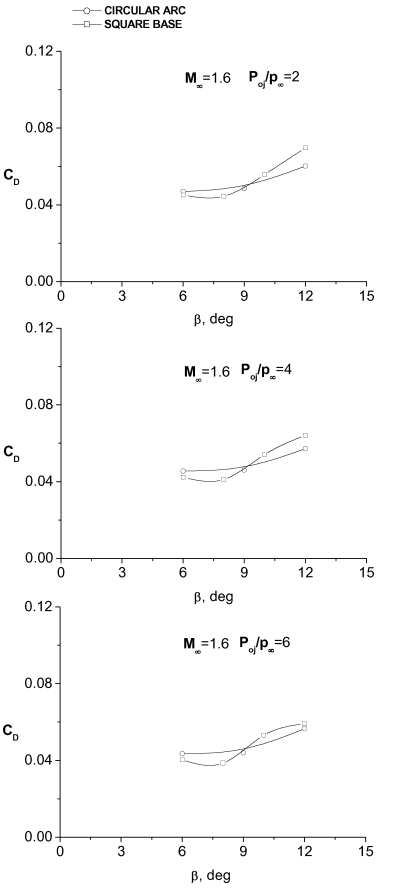

Fig. 11 Comparison of total drag characteristics of circular-arc and square-base afterbodies: $M_\infty = 1.60$.

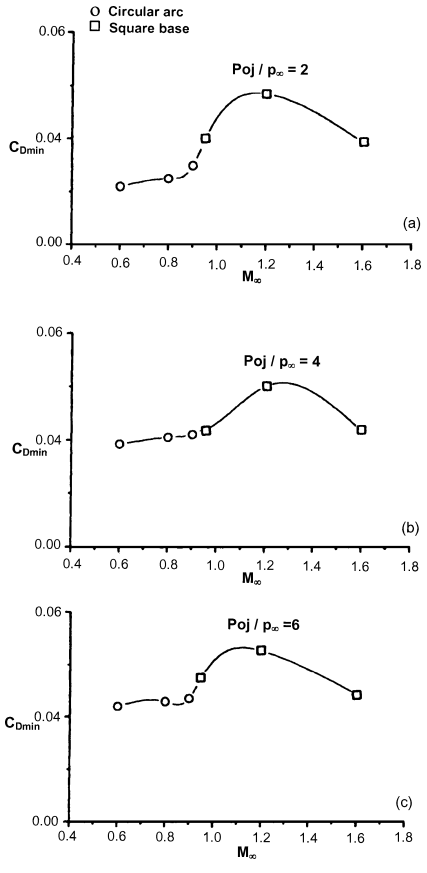

Fig. 12 Globally minimum afterbody total drag at different Mach numbers and jet pressure ratios.

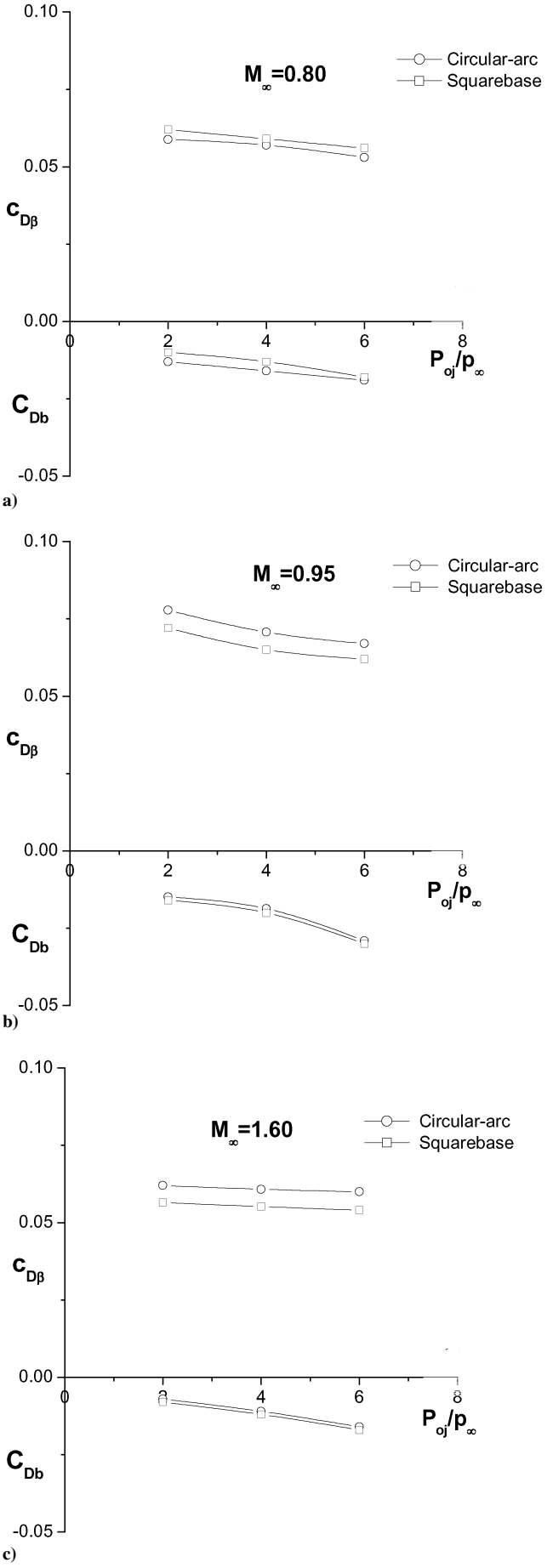

Fig. 13 Comparison of boat-tail and base-drag characteristics of circular-arc ($\beta = 9$ deg) and square-base ($\beta = 8$ deg) afterbodies.

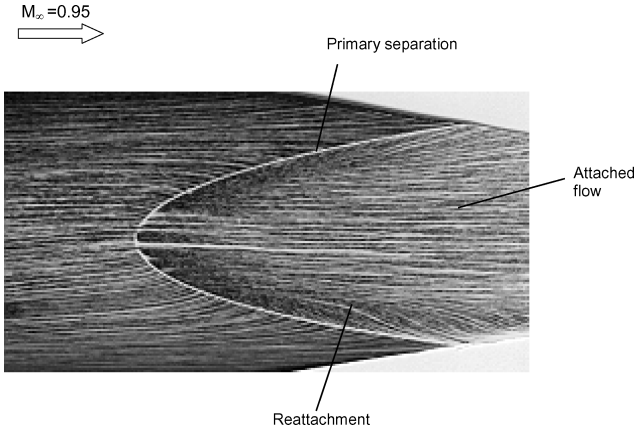

Fig. 14 Typical surface flow features on a square base with jet flow: $M_\infty = 0.95$, $\beta = 8$ deg, and $P_{oj}/p_\infty = 6$.

circular-arc ($\beta = 9$ deg) and square-base ($\beta = 8$ deg) afterbodies, are presented; the results are shown for three values of jet pressure ratio. At $M_\infty = 0.80$ where the globally minimum drag configuration is the circular-arc afterbody (Fig. 12), the results (Fig. 13a) show that values of both $C_{D\beta}$ and C_{Db} are lower compared to the square base. At $M_\infty = 0.95$ and 1.60, the results (Figs. 13b and 13c) show that the boat-tail profile drag $C_{D\beta}$ is appreciably lower for the square-base compared to circular-arc boat tail, with the base thrust component remaining nearly the same; the results were similar at $M_\infty = 1.20$ as well. The preceding results indicate that the total drag reduction associated with the square base is caused primarily by the relatively lower boat-tail pressure drag (changes in skin-friction drag assumed small because the wetted areas are nearly the same for all cases) on them, suggesting strong jet plume displacement effects (compared to the circular-arc boat tails).

D. Broad Flow Features and Surface-Pressure Distributions on a Square-Base Afterbody

As discussed earlier, vortex flows are generated on the four inclined flat segments of a square-base afterbody. An example of such a flow feature, obtained from surface flow-visualization technique, is displayed in Fig. 14 for the optimum β of 8 deg at $M_\infty = 0.95$ and $P_{\mathrm{oj}}/p_\infty = 6.0$. Features like primary separation, reattachment, and attached flow zones on the flat segment can be observed. Vortex flow is generated by the separation of the boundary layer along the U-shaped surface discontinuity; the larger the value of β, the higher will be the strength of the vortex formed, as on delta wings as incidence is increased.

Typical longitudinal and spanwise surface-pressure distributions measured on the inclined flat segment for the preceding case of $\beta = 8$ deg at two Mach numbers of 0.95 and 1.20 are presented in Fig. 15; the longitudinal and spanwise distances are normalized by the length of the flat segment L and delta-wing surface span C, respectively, as indicated in Fig. 15. The spanwise C_p distributions do reveal low pressures associated with vortex flow, and the pressure levels increase appreciably with jet pressure ratio P_{oj}/p_∞. The longitudinal pressure distributions, again, indicate significantly increased pressure recovery with jet pressure ratio. These results indicate significant reduction in boat-tail pressure drag $C_{D\beta}$ as affected by jet pressure ratio and so consistent with observations made from balance measurements (Fig. 13). The increased surface-pressure levels on the inclined flat segment of the square base with jet pressure ratio again suggest strong jet plume displacement effect on these afterbodies.

As discussed in the preceding sections, the flow features on a square-base afterbody are quite complex involving three-dimensional vortex flows (like a delta wing at incidence), subsequent three-dimensional boundary-layer separation at the base and jet interaction. Essentially, the flowfield is highly viscous dominated and three-dimensional. Additional studies involving flowfield measurements (e.g., using particle image velocimetry) and

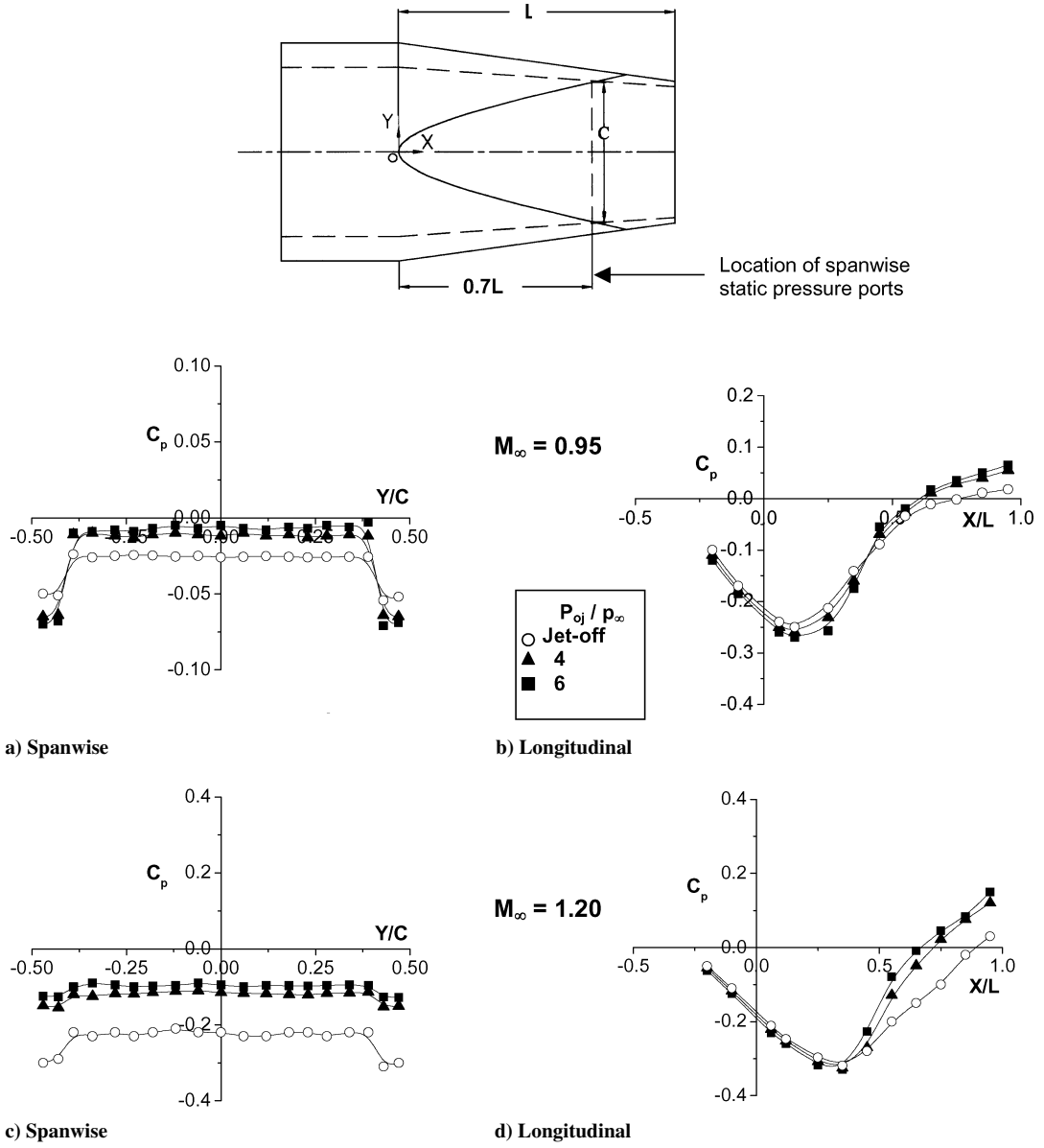

Fig. 15 Typical streamwise and spanwise surface-pressure distributions on a square-base afterbody: $\beta = 8$ deg.

Reynolds-averaged Navier–Stocks calculations could result in a better understanding of mechanisms leading to drag reduction on a square-base afterbody.

IV. Conclusions

A systematic parametric study examining the zero-lift drag characteristics of a family of square-base afterbodies in the presence of sonic jet flow at the base has been carried out in the 0.5-m special-purpose base flow wind tunnel. Accurate measurements of afterbody total drag have been made using a special balance. It has been demonstrated for the first time that, compared to conventional axisymmetric boat tailing with conical and circular-arc profiles (having the same base area and jet exit area), the square-base afterbodies have the lowest total drag in the Mach-number range of 0.95–1.60 at different values of jet pressure ratio: the total drag reduction observed is about 10–12% (relative to circular-arc boat tails) in the range of Mach number and jet pressure ratio examined and can be of significant value in design applications. The passive surface shaping associated with the square-base afterbody results in two broad effects: 1) in the formation of vortex flows on the flat segments, which can be expected to energize the flow on the afterbody (like a vortex generator) leading to greater resistance to plume-induced boundary-layer separation and thereby lower transonic drag rise; and 2) a significant reduction in the boat-tail pressure drag caused by strong jet-plume displacement effect. It would seem rather natural to exploit the passive afterbody shaping of the kind examined here on nonaxisymmetric afterbodies relevant to twin jet aircraft configurations.

Acknowledgments

The authors are thankful to Aeronautics Research and Development Board, Government of India for funding this project. The authors greatly appreciate efforts of staff of base flow tunnel, in particular the help of R. Ramesh in conducting the experiments.

References

[1]Capone, F. J., "Aero-Propulsion Characteristics at Mach Numbers upto 2.2 of Axisymmetric and Non-Axisymmetric Nozzle Installed on an F-18 Model," NASA TP 2044, Aug. 1982.

[2]Hilly, P. J., Eallace, H. W., and Booz, D. E., "Non-Axisymmetric Nozzles Installed in Advanced Fighter Aircraft," *Journal of Aircraft*, Vol. 13, No. 12, 1976, pp. 1000–1006.

[3]Capone, F. J., "The Non-Axisymmetric Nozzle It Is for Real," AIAA Paper 79-1810, Aug. 1979.

[4]Wilmoth, R. G., and Putnam, L. E., "Subsonic/Transonic Prediction Capabilities for Nozzle/Afterbody Configurations in Numerical Methods for Engine-Air Frame Integration," edited by S. N. B. Murthy and

G. C. Payenter, Progress in Astronautics and Aeronautics, Vol. 102, AIAA, Washington, DC, Jan. 1986, pp. 401–430.

[5]Viswanath, P. R., and Patil, S. R., "Drag Characteristics of Class of Non-Axisymmetric Afterbody at High Speeds," National Aerospace Lab., Rept. PD EA 9407, Bangalore, India, April 1994.

[6]Viswanath, P. R., and Patil, S. R., "Zero-Lift Drag Characteristics of Afterbodies with a Square Base," *Journal of Spacecraft and Rockets*, Vol. 34, No. 3, 1997, pp. 290–293.

[7]Platou, A., "Improved Projectile Boat-Tail," *Journal of Spacecraft and Rockets*, Vol. 12, No. 12, 1975, pp. 727–732.

[8]Mathur, N. B., Ramesh, R., and Ramesh, G., "Calibration Studies in the High Speed Base Flow Wind Tunnel," National Aerospace Lab., Rept. PD EA 9804, Bangalore, India, April 1998.

[9]Krishnan, V., and Mathur, N. B., "Afterbody Boundary Layer Measurements in the Base Flow Wind Tunnel," National Aerospace Lab., Rept. PD EA 9705, Bangalore, India, March 1997.

[10]Mathur, N. B., Verma, R. S., and Ramesh, R., "A Test Technique for the Direct Measurement of Afterbody Drag in the Presence of Jet Exhaust," *Proceedings of the 51st Annual General Body Meeting of Aeronautical Society of India*, Hyderabad, India, 2000.

[11]Mathur, N. B., Verma, R. S., and Ramesh, R., "Development of the Test Technique for the Direct Measurement of Afterbody Drag in the Presence of Jet Exhaust in the Base Flow Wind Tunnel," National Aerospace Lab., Rept. PD EA 9803, Bangalore, India, May 1998.